

Ship Silhouette Recognition Using Principal Components Analysis *

V. Gouaillier¹ and L. Gagnon²

¹Département de Math. et Stat., Univ. de Montréal, C.P. 6128 Succ. Centre-Ville, Montréal(Québec), H3C 3J7, CANADA

²Département de R&D, Lockheed Martin Canada Inc., 6111 Ave. Royalmount, Montréal(Québec), H4P 1K6, CANADA

ABSTRACT

We report on an evaluation study of a ship classifier based on the Principal Components Analysis (PCA). A set of ship profiles are used to build a covariance matrix which is diagonalized using the Karhunen-Loève transform. A subset of the principal components corresponding to the highest eigenvalues are selected as the ship features space. The recognition process consists in projecting a profile on this eigen-subspace and performing a similarity measure (herein a standard Euclidean distance). We have measured the recognition performance of the classifier using various sets of range-profile signatures of ship silhouette images and simulated synthetic aperture radar images of ships under various aspect angles. It is found that the PCA-based ship classifier design offers good class discriminacy when trained with a limited number of ship classes (< 10) under an aspect angle range of 60 degrees about the ship side view. Additional tests are however necessary to validate the classifier on larger data sets and real images.

Keywords: Target Recognition, Automatic Ship Classification, Principal Components Analysis, Synthetic Aperture Radar

1. INTRODUCTION

The aim of this paper is to present preliminary results of a feasibility study about the use of the Principal Components Analysis (PCA) for the automatic classification of ships.

Due to the increasing technological advance of imaging sensors like the Forward Looking Infra-Red (FLIR) sensors and the Synthetic Aperture Radar (SAR), the design and implementation of automatic ship recognition systems are getting much interest in the scientific and engineering communities. However, despite the fact that automatic ship recognition brings out interesting scientific challenges, very few results are reported in the open literature¹⁻¹². This is probably caused by the difficulty of accessing real image data due to the potential strategic interest of this research field. Many works about automatic ship recognition are performed under classified military contracts (see, for example, Ref. 13 and references therein).

1.1 Framework

Lockheed Martin Canada (LM Canada) has engaged internal R&D activities in automatic ship recognition over the last 2 years, in collaboration with University partners⁷⁻⁹. These researches are part of the LM Canada R&D program in airborne sensor fusion with targeted applications in ocean and coastal surveillances^{7-9,14-16}. Up to now, we have concentrated our effort on the problem of feature extraction and classification of ships from SAR images and subsequent fusion with non-imaging sensors in order to improve long-range target identification within a Command and Control System (CCS)¹⁴.

Figure 1 illustrates the system design LM Canada is currently studying for ship feature extraction and recognition from Spotlight SAR (SSAR) or Inverse SAR (ISAR) images. Both target features and identification are sent to a fusion system (that uses the Dempster-Shafer evidential reasoning approach), following a four-step hierarchical structure and through small dedicated modular classifiers. This hierarchical approach has numerous advantages: (1)

*SPIE Proc. #3164, conference "Applications of Digital Image Processing XX", San Diego, 1997

low technical risk due to the use of pattern recognition algorithms of increasing complexity, (2) easier system design refinement and upgrade, (3) incremental implementation and (4) easier and more efficient retraining procedures than for large classifiers.

The preliminary target detection step and the subsequent SAR antenna orientation are assumed to be performed with the help of the range-bearing information provided by the conventional radar mode. At the operator request, a potential ship target is imaged at high resolution using the SSAR or ISAR modes. For now, we assume that the SAR image generator provides adequate platform and target motion compensations to assure minimal blurring effects in the image (otherwise, this can impose a severe limit in the classification performance). The resulting target image, along with the target range (slant-range), the platform altitude and the target aspect angle (which could be acquired from a previous long tracking time), constitute the input data for the system.

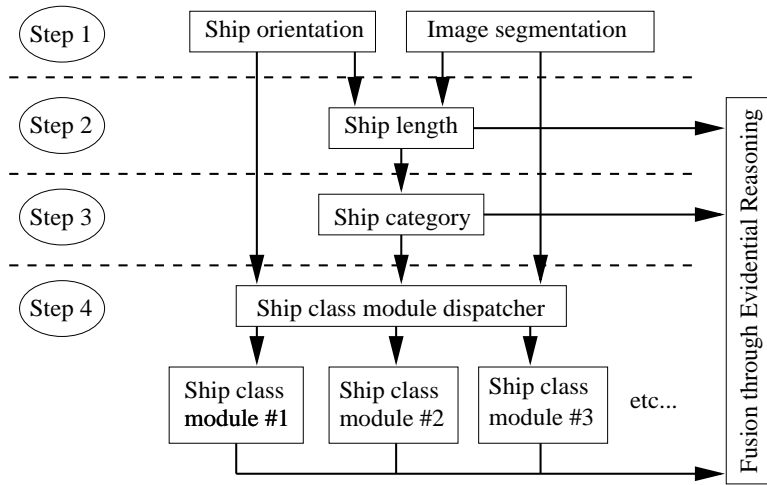


Figure 1: Hierarchical ship classifier design under study at LM Canada

Step 1 in Figure 1 consists in segmenting out the target pixels from the ocean clutter. Two algorithms have been implemented and tested for that purpose. The first is based on a neural clustering scheme, called Probabilistic Winner-Take-All (PWTA), which aims to provide a neural approximation to the optimal Bayesian clustering⁷. As opposed to the standard K-means algorithms, the PWTA adapts the means and the variances of the clutters, which provides a better representation of the input distribution. The second segmentation algorithm is based on a combination of directional pixel intensity thresholding (in order to remove linear strikes and artifacts caused respectively by rotating ship antenna and/or SAR image generator defects) followed by morphological operations that eliminate small non-connected regions and merge large ones.

Step 2 aims to calculate the ship length, which is a simple but very discriminating feature in ship classification. Ship length is calculated by identifying the target’s end-points and using their respective coordinate information in the SSAR or ISAR image-plane geometry formula. Following Musman et al., ship end-points are obtained by estimating the ship center-line from the maximum peak of the Hough transform of the segmented image^{4,14}. This technique works well on targets of high eccentricity, which is the case for elongated objects like ships when imaged under appropriate geometry (which is different for optical and radar sensors). If the ship is classified as "large ship" (lets say, ship length above 70 m), then the original image is sent to the first target classification step (Step 3); otherwise it is labeled as small ship and not analyzed further (our current ship data-base does not contain small ships yet). A "small ship" declaration can also be caused by (1) a failure in the segmentation step (2) a lack of ship profile or plan information in the image or (3) a failure in the ship end-points detection.

Step 3 is the first target classification step in the hierarchy. It has been designed to provide a high-level identification declaration of the ship category, that is military or merchant ship. This classification is based on the spatial distribution of radar scattering along 9 sections of the ship target¹³; military (more precisely military combatant ships such as frigate, destroyer, cruiser) have large structures, thus radar scattering, concentrated in the middle

part of the ship while merchant ships (e.g. cargo, tanker) radar scattering comes mainly from the ship end regions. Because of a limitation in the number of real data, a set of 9-dimensional scatterer distributions have been simulated and used to train and validate a 3-layer back-propagation Neural Net (NN) with an expert-system supervisor. Tests were made with real data only. The NN has 3 outputs corresponding to combatant, merchant or unknown. The outputs are normalized to provide a confidence level associated to the declaration (the sum of all confidence levels is 100%). Ship length and ship category, along with the associated confidence levels, are sent to the fusion module where all sensor declarations and features are processed using a truncated Dempster-Shafer evidential reasoning algorithm^{17,18}. Detail results about the above will be reported soon.

1.2 PCA-based classifier module

If a more accurate target identification is required, like ship type (e.g. frigate, destroyer, cruiser, cargo, tanker) or even ship class (e.g. Mackenzie-class frigate, Belknap-class cruiser), and if the confidence level on the ship category is sufficiently high (e.g. 85%), then the last step (Step 4) in the ship recognition process is engaged. This necessitates much more sophisticated classifiers in order to encode small differences in ship features^{3,6-9,13}. Rather than training a large NN classifier that would most probably lead to convergence problems (a typical ship database for surveillance activities might contain up to 1000 ships, imaged at 180 different aspect angles and 13 depression angles), we are considering a modular approach consisting of many small dedicated classifiers, each of them being specialized to recognize a subset of the ship database under a small viewing angle range. This approach has also the advantage of avoiding the training of a large classifier if a new ship is entered in the database. During the recognition process, only modules corresponding to the radar viewing angle and the most probable ship classes would be fired. This information might be obtained from the fusion system which has the capability of providing a list of the most probable target identifications.

The PCA-based algorithm is one of the proof-of-concept ship module classifiers that are currently tested by one of our University collaborators⁹. The other classifier design under study is a kind of multi-resolution back-propagation neural network for which test results will be reported elsewhere⁸.

The principal components transform (also known as Karhunen-Loève or Hotelling transforms) is a linear operation that transforms a set of data into a new orthogonal set and provides a feature selection mechanism under the minimization of a Mean Square Error (MSE) criteria¹⁹. This last property results from the inherent PCA encoding scheme that orders data information according to the eigenvalues of the covariance matrix of the ensemble data; eigenvectors having larger (lower) eigenvalues encode coarse (fine) information. Altogether, properties that make PCA attractive to features extraction and classification problems are

- distribution structure (metric) conservation due to the orthogonality of the transform,
- data decorrelation,
- coarse-to-fine information ordering,
- data compression that minimizes the MSE,
- automatic low-dimensional feature vector selection
- fast unsupervised training.

PCA is a very popular tool in image processing, especially in the representation, preprocessing and orthogonal coding of multi-spectral imagery. It is used, for example, in artificial coloring scheme, in classification of vegetation and in noise estimate of SAR images. It has found one of its most important applications in the field of target image classification with the works of Sirovich & Kirby²⁰ and Turk & Pentland²¹ about face recognition. The success encountered there²² has been the source of motivation of other PCA-based target image classification works²³⁻²⁴ as well as of the present study.

2. PCA CLASSIFICATION ALGORITHM

The PCA-based classification algorithm can be divided in two steps: initialization (training) and recognition (testing). Briefly, the initialization step aims at performing a PCA on a set of training vectors (e.g. images, range-profiles, etc.) and determining a subset of eigenvectors (principal components) that best account for the distribution of all vectors within the space. These eigenvectors are used to encode low-dimensional feature vector distributions corresponding to the different target classes. The recognition step consists in projecting a test data on the selected principal components followed by a similarity measure for identifying the data class.

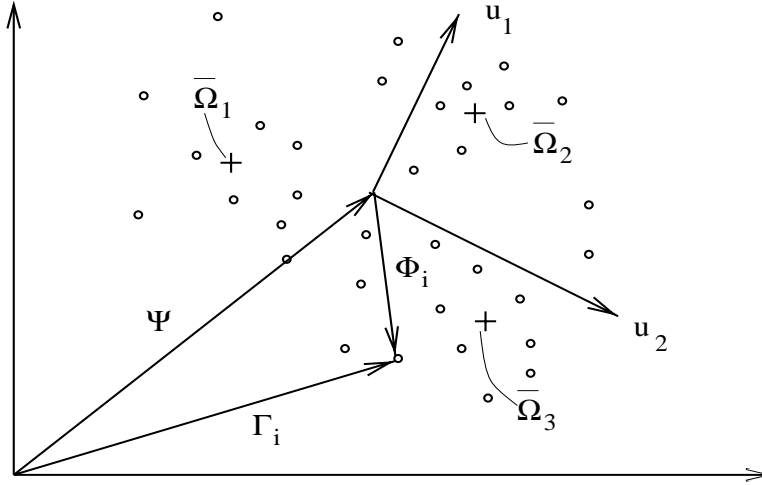


Figure 2: Example of a Karhunen-Loève transform for a 3-classes case.
(M is the number of points and $N = 2$ in this sketch)

The training step can be summarized as follows²¹ (One can refer to Figure 2 for a geometrical interpretation).

- Select a set of M training vectors $,_i$ ($i = 1, \dots, M$) of dimension N .
- Calculate the mean vector $\Psi = \frac{1}{M} \sum_{i=1}^M ,_i$ and the centered vectors $\Phi_i = ,_i - \Psi$.

This operation translates the origin of the raw data coordinates axes to the origin of the principal axes distribution which is necessary to minimize the MSE in the principal component development¹⁹. The centered vectors Φ_i are subject to the PCA which seeks a set of orthonormal vectors u_i (the principal components) which best describes the data distribution. Under the MSE minimization criteria, imposed on the principal component expansion, one can show that these vectors correspond to the eigenvectors of the covariance matrix $C = \frac{1}{M} A A^T$, where A is the matrix defined as $A = (\Phi_1, \Phi_2, \Phi_3, \dots, \Phi_M)$, having the largest eigenvalues. The dimension of C is $N \times N$. If N is large the calculation of the eigenvectors might be untractable (for instance, if the training vectors are 128x128 pixels images, then $N = 16384$). One can reduce the computational load by working with the matrix $L = \frac{1}{M} A^T A$ which is of dimension $M \times M$ (we will see later that $M \ll N$ in our application). In fact, one can show that if v_i is eigenvector of L , then $A v_i$ is eigenvector of C . Thus, C has at most M non-vanishing eigenvalues (Actually, C has at most $M - 1$ eigenvectors, due to the linear dependence introduced by the mean translation).

- Calculate the eigenvectors v_i and eigenvalues λ_i of L .
- Select M' eigenvectors that correspond to the M' largest eigenvalues ($M' < M$).

This process encodes the data information in a feature space of dimension M' . The eigenvectors having the highest eigenvalues correspond to data information that has the largest variance (the coarse information) while

the eigenvectors having the lowest eigenvalues contain detailed information that does not contribute significantly to the feature space. The choice of M' is based on a trade-off between the wanted system performance and the data Compression Ratio (CR) which we will label by the ratio M'/M . A large CR reduces the feature space dimension but might limit the classification performance. A low CR is not always necessary. In practice, CR is determined empirically.

- Normalize the principal components as $u_i = Av_i/|Av_i|$
- Finally, calculate the cluster parameter distribution for each object class represented in the training set.

In this work, we characterize each cluster distribution by the cluster center $\bar{\Omega}$ of coordinates $(\bar{\omega}_1, \bar{\omega}_2, \dots, \bar{\omega}_{M'})$, where $\bar{\omega}_k = \overline{\langle \Phi_i, u_k \rangle}$ is the average of all the projections onto the k^{th} eigenvector, over the subset of all training vectors Φ_i that belong to one specific class. This cluster center constitutes the feature vector representative for each class.

The recognition step can be summarized as follows. Let Φ be a test vector to be identified.

- Translate the test vector by the mean training vector Ψ (i.e. $\Phi = \Phi - \Psi$).
- Calculate the feature vector $\Omega = (\omega_1, \omega_2, \dots, \omega_{M'})$, where $\omega_k = \langle \Phi, u_k \rangle$.
- Reconstruct the test vector from the truncated eigenvector expansion using $\Phi_{reconst} = \sum_{k=1}^{M'} \omega_k u_k$.
- Calculate the distances $\varepsilon_{reconst} = |\Phi_{reconst} - \Phi|$ and $\varepsilon_i = |\Omega - \bar{\Omega}_i|$ which are the reconstruction and class errors respectively.

The identification process itself consists in associating the feature vector Ω to one of the class clusters. This can be done under various association scenarios (e.g. probabilistic, minimum distance). Both errors $\varepsilon_{reconst}$ and ε_i can be used in the identification process. One can determine a space threshold $\theta_{reconst}$ that can serve as a decision boundary as to whether a test vector Φ belongs or not to the vector space. (This can be used in practice to decide if an input object “looks like” a ship or has a global aspect that makes it similar enough to the truncated training ship space). One can also determine a class threshold θ_i for each cluster i and identify a vector Φ to class i only if $\varepsilon_i < \theta_i$. This can be done empirically or statistically if one has enough data samples for each class. For now, we concentrate on the simple minimum distance classification which associates an input test vector to the nearest class provided the space error $\varepsilon_{reconst}$ is below an empirically determined threshold. Minimum distance association is a valuable method when the number of training samples is limited as it is the case here.

3. TESTS

We have performed 2 types of tests in this study. The first type aims at estimating the classifier robustness with respect to systematic target deformations. The second type aims at quantifying the recognition performance on simulated SAR images. Following face recognition nomenclature²¹, the two efficiency measures we have used are the Recognition Rate (RR) and the False Acceptance Rate (FAR). The RR refers to how successful is the classifier to recognize a ship for which samples have been presented to the classifier during the training set (RR should be as high as possible). The FAR measures the robustness of the classifier to discard targets that have not been used in the training set (FAR should be as low as possible). Low FAR helps in keeping a high confidence level on the classifier declaration. Of course, there is a trade-off between both types of errors and consequently it is much more difficult to build a system with a high RR and a low FAR than a system with a high RR alone.

Following many other authors^{2,4,6,13}, we have decided to use the target range-profile as the input vector for the PCA-classifier. Range-profile is a standard 1-D signature in target SAR imaging which is obtained by summing pixel intensities along the Doppler (or cross-range) axis (usually the image columns). PCA-based target classifier can also be implemented directly on the images^{21,23,24} but it is not clear whether it would offer a clear advantage here; especially for ISAR images where the cross-range target spreading is highly dependent on the target motion.

However, we recognize that the range-profile could introduce a degeneracy (two different ships could have the same range profile), especially when one works on binary segmented images, but this is very unlikely for small databases.

For the first type of tests, we have used two sets of military ship silhouettes having ship lengths in the range 100-150 m. The following test have been performed:

- Test 1a: Training with 10 ship classes (one representative for each class). Test (confusion matrix) with the same ship classes with images modified under 8 systematic deformations (80 deformed ship images in total).
- Test 1b: Training with 10 ship classes (one representative for each class). Test (RR and FAR) with 26 ship classes from which 10 (the training class ship representatives) are modified by 7 systematic deformations (86 test images in total). The RR is calculated from the 70 deformed ships and the FAR from the 16 other non-deformed ships.
- Test 1c: Training with 30 ship classes (one representative for each class). Test (RR and FAR) with 50 ship classes from which 30 (the training class ship representatives) are modified by 7 systematic deformations (230 test images in total). The RR is calculated from the 210 deformed ships and the FAR from the 20 other non-deformed ships.

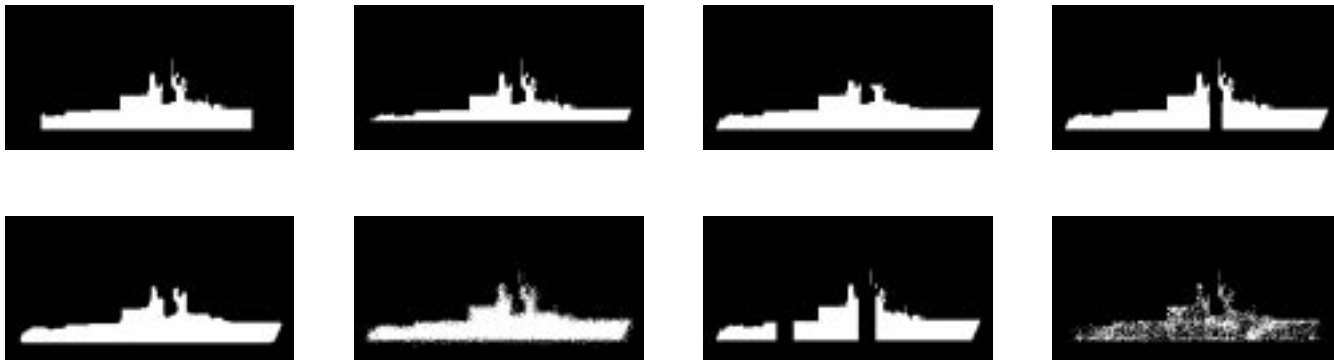


Figure 2: Example of systematic deformations considered in Test 1a-c.
Deformations #1 to #4 are on the first row.

Considered deformations are shown on Figure 2. These include bow and stern occlusions, hull occlusion, small features removal, one band mask in the ship center part (between two ship structures if possible), ship contour smoothing, ship contour spreading, two-bands mask and impulse noise. Such deformations mimic various characteristics of SAR images of ships¹³ such as absence of radar scattering for specific target orientations, poor scattering properties of ship end-points and speckle noise. Deformations #1 to #8 are used in Test 1a; deformations #1 to #7 are used in Tests 1b and 1c.

Results of Test 1a are summarized in the confusion matrices of Table 1. The first column gives the actual ship class number while first row refers to the ship class reported by the classifier. The principal numbers indicate the number of reports with subscripts referring to the deformations (1 to 8). Two different data compression ratios have been tested: 4/10 and 9/10 principal components retained. In these experiences, no space threshold has been fixed because no FAR measure is performed. Only the 8 deformations of the 10 training ships (10 ship classes) are presented to the classifier. Confusion matrices show that even for the low CR (9/10), almost all noisy ships (deformation #8) are mis-classified. Unlike the other deformations, the spray effect introduces a global range profile deformation that affect information at all levels (coarse and fine). In fact, PCA is very sensitive to low-frequency perturbations, which is the result of the coarse-to-fine information encoding process. When applied to SAR images, one thus has to make sure that the image generator has a fairly constant signal-to-noise ratio in order to limit degradation of the PCA classification performance. On the other hand, PCA is less sensitive to absence of few scatterers or bad ship end-points imaging.

	1	2	3	4	5	6	7	8	9	10
4/10 Principal Components										
1	3 _{3,5,6}							1 ₁		4 _{2,4,7,8}
2		7 ₁₋₇								1 ₈
3			7 ₁₋₇							1 ₈
4				6 ₂₋₇				1 ₁		1 ₈
5					7 ₁₋₇					1 ₈
6				2 _{2,8}		6 _{1,3-7}				
7	4 _{1,3,4,7}						2 _{5,6}			2 _{2,8}
8				1 ₄				4 _{1,3,5,6}		3 _{2,7,8}
9									7 ₁₋₇	1 ₈
10										8 ₁₋₈
9/10 Principal Components										
1	7 ₁₋₇			1 ₈						
2		7 ₁₋₇		1 ₈						
3			7 ₁₋₇	1 ₈						
4				7 ₁₋₈						
5				1 ₈	6 _{1,3-7}		1 ₂			
6				1 ₈		7 ₁₋₇				
7				1 ₈			7 ₁₋₇			
8				2 _{2,8}				7 ₁₋₇		
9				1 ₈					7 ₁₋₇	
10										8 ₁₋₈

Table 1: Confusion matrix for Test 1a with 4/10 (upper) and 9/10 (lower) principal components retained. The RR are 71% and 87% respectively

Tables 2 and 3 show the classifier performances obtained for Tests 1b and 1c, respectively. Three different data compression ratios have been tested: 2/10, 4/10 and 9/10 principal components retained for Test 1b and 7/30, 14/30 and 29/30 for Test 1c. We report the RR obtained when the space error is below an empirically determined threshold and when the classifier correctly identifies the target among the one (Top 1), two (Top 2) or three (Top 3) lowest classifier outputs (surveillance operators do not usually rely on single output automatic recognition systems). The FAR is measured by presenting ship targets never seen by the classifier. A false acceptance is then recorded when the space error is below the space threshold. We report recognition performances for low FAR only; numbers depicted in Tables 2 and 3 correspond to the best RR obtained when varying the space threshold while keeping the FAR to 0%, 10% and 20%. Of course, better RR can be obtained by relaxing the low FAR requirement.

	2/10 PC			4/10 PC			9/10 PC		
	Top 1	Top 2	Top 3	Top 1	Top 2	Top 3	Top 1	Top 2	Top 3
RR (%) @ 0% FAR	30	34	34	33	37	37	40	44	44
RR (%) @ 10% FAR	34	38	39	53	57	60	67	73	73
RR (%) @ 20% FAR	46	56	57	73	78	84	74	80	80

Table 2: Recognition performances for Test 1b

Test 1c yields yet lower RR, which might reflect a limitation of our current PCA classifier, regarding the number of similar ships it can discriminate when only one representative per class is used. The 30 ships used in the training set are all military ships and apart from the ship length, frigates, destroyers and cruisers have quite a similar appearance (main structures concentrated on the ship central part). Increasing the number of representatives for each ship class is necessary to improve the classification performance when increasing the number of ship classes.

	7/30 PC			14/30 PC			29/30 PC		
	Top 1	Top 2	Top 3	Top 1	Top 2	Top 3	Top 1	Top 2	Top 3
RR (%) @ 0% FAR	9	9	10	19	19	19	30	31	31
RR (%) @ 10% FAR	24	28	29	46	50	52	57	59	59
RR (%) @ 20% FAR	43	48	50	52	56	59	68	70	70

Table 3: Recognition performances for Test 1c

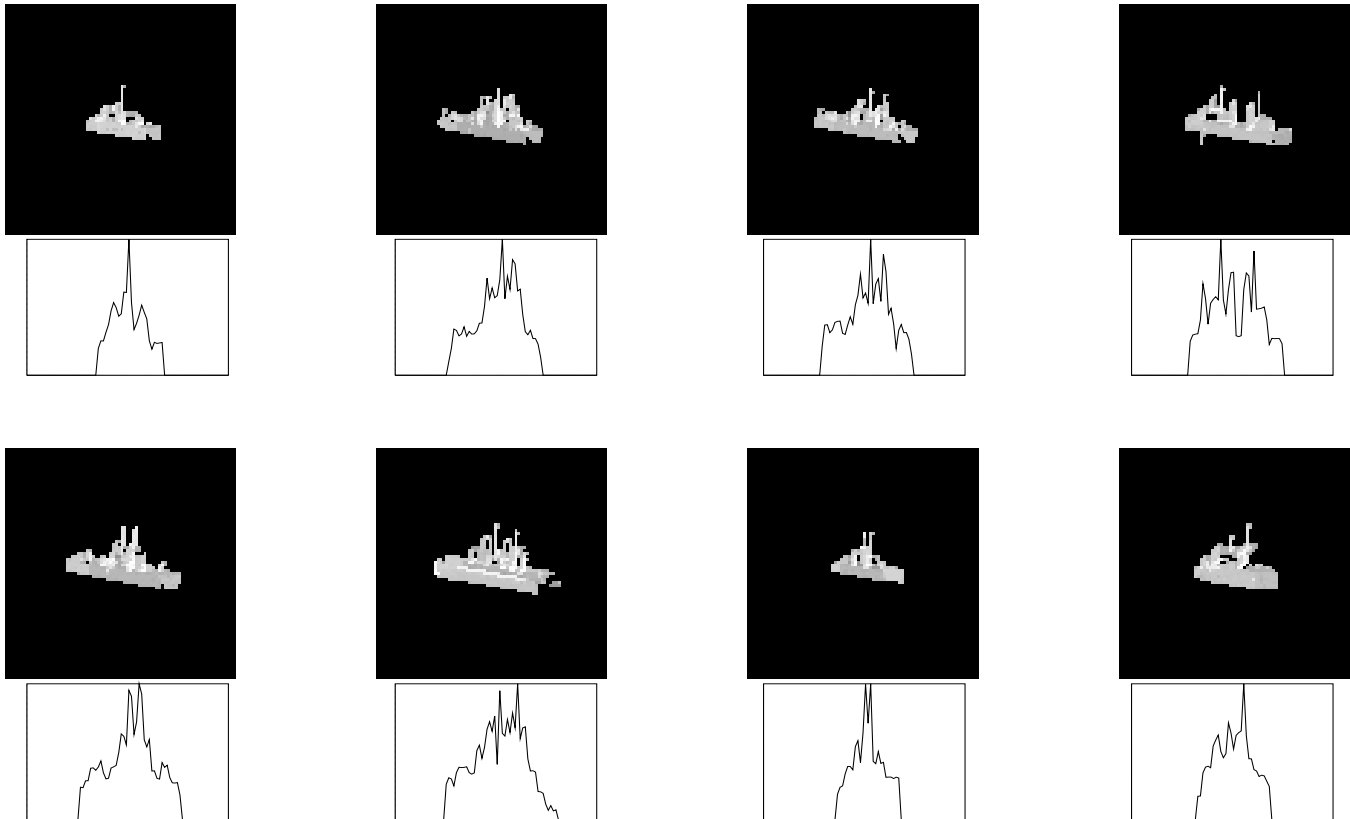


Figure 3: Examples of simulated SAR images used in Test 2a-d. Curves show the target range-profiles. Ship classes #1 to #4 are on first row.

The second type of tests was aimed at quantifying the recognition performance on simulated SAR images of ships. We have used a set of 202 simulated SAR images of 8 ship classes with a ship length range of 112-170 m. Each classe contained 24 images generated 2.5 degrees apart from 60-120 degrees with respect to the ship heading (i.e. the aspect angle range is ± 30 degrees from the ship side view). The radar platform depression angle was set to about 2 degrees during the simulation and the image resolution has been kept constant for all images. Image samples are given in Figure 3. Pixel values have all been normalized between 0 and 255. The horizontal and vertical directions are the range (more precisely the slant-range) and cross-range coordinates with respect to the radar line-of-sight.

The following experiences have been performed:

- Test 2a: Training with 4 ship classes (#2, 3, 4 and 5) with 6 odd-numbered images/class (24 in total) covering a 30 degrees aspect angle range (images 5 degrees apart). Test (RR and FAR) with 8 ship classes with 6 even-numbered images/class (48 in total).
- Test 2b: Training with 4 ship classes (#2, 3, 4 and 5) with 12 odd-numbered images/class (48 in total) covering

a 60 degrees aspect angle range (images 2.5 degrees apart). Test (RR and FAR) with 8 ship classes with 12 odd-numbered images/class (96 in total).

- Test 2c: Training with the 8 ship classes with 6 odd-numbered images/class (48 in total) covering a 30 degrees aspect angle range (images 5 degrees apart). Test (RR only; no space threshold set) with 8 ship classes with 6 even-numbered images/class (48 in total).
- Test 2d: Training with the 8 ship classes with 12 odd-numbered images/class (96 in total) covering a 60 degrees aspect angle range (images 2.5 degrees apart). Test (RR only; no space threshold set) with 8 ship classes with 12 even-numbered images/class (96 in total).

	5/24 PC			10/24 PC		
	Top 1	Top 2	Top 3	Top 1	Top 2	Top 3
RR (%) @ 0% FAR	75	79	83	75	79	87
RR (%) @ 10% FAR	79	87	96	79	87	96

Table 4: Recognition performances for Test 2a

	10/48 PC			20/48 PC		
	Top 1	Top 2	Top 3	Top 1	Top 2	Top 3
RR (%) @ 0% FAR	40	46	60	43	60	67
RR (%) @ 10% FAR	56	65	77	52	71	81

Table 5: Recognition performances for Test 2b

Tables 4 and 5 show the classifier performance obtained for Tests 2a and 2b, respectively. Two different data compression ratios have been tested: 5/24 and 10/24 principal components retained for Test 2a and 10/48 and 20/48 for Test 2b. Better recognition rates are obtained here than in Tests 1. Two facts contribute to this: smaller number of ship classes and more ship representatives per class (imaged at slightly different viewing angles). The data compression capability of the PCA is also apparent from the small difference in the RR results between the high and low CR; the high CR has encoded enough information to yield good recognition performance.

	4/48 PC			10/48 PC			20/48 PC		
	Top 1	Top 2	Top 3	Top 1	Top 2	Top 3	Top 1	Top 2	Top 3
RR (%) (no FAR measured)	52	73	98(?)	58	75	89	63	75	89

Table 6: Recognition performances for Test 2c

Results of Tests 2c and 2d are yet more explicit on the compression capacity of the PCA approach (Tables 6 and 7). There, three different data compression ratios have been tested on a 8-classes PCA classifier. No FAR has been measured here which makes RR results valid only for recognition applications involving only these 8 target classes. Apart from the peculiar 98% RR obtained in Test 2c, there is an obvious stability in the classifiers performances over the 3 compression ratios. This clearly illustrates one of the motivation in using the PCA approach, that is, the possibility of increasing the data compression ratio (i.e. keep only a small subset of the principal components) without affecting too much the RR. On the other hand, the lower performance obtained here, in comparison to Tests 2a and 2b, is probably caused by the larger ship length variation among the training set. Other experiments we have performed (not reported here) have also shown that the best recognition results are obtained when there is not much length variation in the training set. This is an important point to take into consideration in the design of the PCA-based ship classifier modules (Figure 1).

4. CONCLUSIONS

We have presented preliminary tests regarding the use of the PCA for the representation and automatic classification of ship silhouettes and ship range-profiles from SAR images.

	8/96 PC			20/96 PC			40/96 PC		
	Top 1	Top 2	Top 3	Top 1	Top 2	Top 3	Top 1	Top 2	Top 3
RR (%) (no FAR measured)	49	67	79	48	69	80	49	68	80

Table 7: Recognition performances for Test 2d

The selection of the PCA approach was motivated by (1) the simplicity of the classification algorithm and (2) the optimal data encoding process with respect to the minimization of the MSE during the data compression (feature extraction). PCA decorrelates the information (removes redundancy by diagonalizing the covariance matrix) and orders it from main tendency to fine details. Additional advantage of the PCA method allows unsupervised and fast training.

Although it is widely recognized that PCA is efficient in encoding and compressing the information, we specifically wanted to verify if it is a good approach for the classification of ship silhouette. Two types of tests have been performed for that purpose: the first estimates the classifier robustness with respect to systematic target deformations and the second quantifies the recognition performance on simulated SAR images of ships. We have used the target range-profile as the input to our classifier and used the simple minimum distance rule for class association. We found that:

- PCA is robust to various local target occlusions and ship contour smoothing but less to global target fade out.
- PCA offers a fair classification performance for medium dimension training sets with only one representative for each ship class; typically 73% RR @ 20% FAR for 10 ship classes (Table 2). However, performance decreases with the increase in the set dimension (Table 3).
- PCA offers a good classification performance for small dimension training sets with more than one representative for each ship class and under a target orientation range of up to 60 degrees; typically 79% RR @ 10% FAR for 4 ship classes (Tables 4 and 5)
- PCA encoding is very efficient for data compression of ship range-profiles through the selection of the principal components having the largest variances (Tables 6 and 7).

There are still open issues that must be addressed before getting a final assessment of PCA-based ship recognition modules (Figure 1). For instance, it is not yet clear how such classifiers will scale to large databases with many ship representatives per class and a large aspect angle range. Also, the space recognition overlapping between classifier modules is still an open question and tests on real SAR images also have to be done. All these issues will be addressed in the future together with a formal comparative study with other ship classifier designs we are currently investigating. These include (1) a multiresolution feed-forward NN that extracts ship features, directly on the image, at three different resolutions⁸ and (2) a linear (non-orthogonal) feature extractor based on class separability criteria defined by a discriminant analysis of within-class, between-class and mixture scatter matrices^{9,19}.

5. ACKNOWLEDGEMENTS

V. G. thanks Prof J. Patera from the Centre de Recherches Mathématiques of the Univ. de Montréal for giving her the opportunity of completing a MSc degree in industry with the help of a student grant from LM Canada and the Natural Sciences and Engineering Research Council of Canada (NSERC). L. G. thanks Prof. S. Blostein and Dr. H. Osman from Queens University for providing the simulated SAR images to LM Canada through an Industry-NSERC grant.

6. REFERENCES

- [1] R. N. Strickland, M. R. Gerber, "Estimation of Ship Profiles from a Time Sequence of Forward-Looking Infrared Images", *Opt. Eng.*, Vol. 25, pp. 995-1000, 1986
- [2] P. E. Zwicke, I. Kiss Jr., "A New Implementation of the Mellin Transform and its Application to Radar Classification

- of Ships", IEEE Trans. Patt. Anal. Mach. Intel., Vol. PAMI-5, pp. 191-198, 1983
- [3] F. Sadjadi, J. O'Sullivan, "Periscope Video Ship Classification", SPIE Proc. #2756, pp. 46-52, 1996
- [4] S. Musman, D. Kerr, C. Bachmann, "Automatic Recognition of ISAR Ship Images", IEEE Trans. Aerospace Electronic Systems, Vol. 32, pp. 1392-1403, 1996
- [5] R. J. Drazovich, F. X. Lanzinger, T. O. Binford, "Radar Target Classification", IEEE, pp. 496-501, 1981
- [6] M. Menon, "An Automatic Ship Classification System for ISAR Imagery", SPIE Proc. #2492, pp. 373-388, 1995
- [7] H. Osman, S. Blostein, "SAR Image Processing Using Probabilistic Winner-Take-All Learning and Artificial Neural Networks", Proc. of IEEE ICIP, Vol. II, pp. 613-616, 1996
- [8] H. Osman, S. Blostein, L. Gagnon, "Classification of Ships in Airborne SAR Imagery Using Backpropagation Neural Networks", (submitted SPIE Proc. #3161, 1997)
- [9] V. Gouaillier, MSc Thesis, Université de Montréal, 1997
- [10] R. D. Klepko, "Automatic Ship Image Extraction from Synthetic Aperture Radar Imagery", Proc. IGARSS'90, 1990
- [11] B. Zvolanek, "Autonomous ship classification by moment invariants", SPIE Proc. #292, pp. 241-248, 1981
- [12] J. J. Kovar, J. Knecht, D. Chenoweth, "Automatic classification of infrared ship imagery", SPIE Proc. #292, pp. 234-240, 1981
- [13] R. D. Klepko, "Automatic Pattern Classification of Airborne SAR Images of Ships", DREO Report #1283 (classified material)
- [14] E. Shahbazian, L. Gagnon, J. R. Duquet, M. Macieszczak, P. Valin, "Fusion of Imaging and Non-Imaging Data for Surveillance Aircraft", SPIE Proc. #3067, 1997
- [15] L. Gagnon, F. Drissi Smaili, "Speckle Noise Reduction of Airborne SAR Images with Symmetric Daubechies Wavelets", SPIE Proc. #2759, pp. 14-24, 1996
- [16] L. Gagnon, A. Jouan, "Speckle Filtering of SAR Images - A Comparative Study Between a Complex-Wavelet-Based and Standard Filters" (submitted for SPIE Proc. #3169, 1997)
- [17] M. A. Simard, E. Boily, J. Couture, "Data Fusion of Multiple Sensors Attribute Information for Target Identity Estimation using a Dempster-Shafer Evidential Combination Algorithm", SPIE Proc. #2759, pp. 577-588, 1996
- [18] E. Bossé, J. Roy, M. A. Simard, "Identity and Attribute Information Fusion Using Evidential Reasoning" (accepted for SPIE Proc. #3067, 1997)
- [19] K. Fukunaga, "Introduction to Statistical Pattern Recognition", (Academic Press, Boston, 1990)
- [20] L. Sirovich, M. Kirby, "Low-Dimensional Procedure for the Characterization of Human Faces", J. Opt. Soc. Amer. A, Vol. 4, pp. 519-524, 1987
- [21] M. Turk, A. Pentland, "Eigenfaces for Recognition", J. Cognitive Neuroscience, Vol. 3, pp. 71-86, 1991
- [22] L. Gagnon, S. Jones, "Computerized Facial Recognition Technology Survey", Lockheed Martin Canada Internal Tech. Report, 1996
- [23] B. D. Singstock, S. K. Rogers, M. Kabrisky, "Automatic Target Recognition Using Karhunen-Loeve Transform Generated Eigenimages", SPIE Proc. #1699, pp. 232-240, 1992
- [24] L. M. Novak, G. J. Owirka, "Radar Target Identification Using an Eigen-Image Approach", Proc. of the IEEE National Radar Conference, p. 129-131, 1994